Original Paper

A molecular dynamics simulation study of paraquat intercalated montmorillonite

Haotian Su[1], Yingchun Zhang[1] ⓘ, Xiandong Liu[1] ⓘ, Qingfeng Hou[2] ⓘ and Xiancai Lu[1]

[1]State Key Laboratory for Mineral Deposits Research, School of Earth Sciences and Engineering, Nanjing University, Nanjing, Jiangsu, China and [2]State Key Laboratory of Enhanced Oil Recovery, Research Institute of Petroleum Exploration and Development, China National Petroleum Corporation (CNPC), Beijing, China

Abstract

Paraquat, one of the most widely utilized herbicides globally, causes a significant environmental challenge due to its poor degradation rate and tendency to adsorb into clay interlayers. Several remediation methods have been proposed but their effectiveness remains suboptimal. The primary reason for this is the lack of microscopic understanding of paraquat–montmorillonite interactions. In this work molecular dynamics simulations were applied to study the interlayer structures and mobility of paraquat intercalated montmorillonite. Two stable hydration states were identified from the calculated immersion energy curve, which corresponded to a water content of 185 mg_{water}/g_{clay} and 278 mg_{water}/g_{clay} (the most stable). Paraquats remained in direct contact with the clay surface in both the anhydrous and hydrated states. At the water content of 185 mg_{water}/g_{clay}, paraquats formed π-π stacking while at 278 mg_{water}/g_{clay}, they were separated by a layer of water. Paraquat showed very small self-diffusion coefficients in the interlayer space of montmorillonite, indicating rather limited motions. The results in this work provide a basis for a better understanding of the interaction of paraquat with clay minerals.

Keywords: hydration state; interlayer structure; mobility; molecular dynamics simulation; montmorillonite; paraquat

Introduction

Paraquat (PQ) (1,1′-dimethyl-4,4′-dipyridylium dichloride) is one of the most widely used herbicides in the world (Santos et al., 2013; Rashidipour et al., 2019). It is favored for its fast-acting, non-selective contact killing of weeds, as well as its inactivation upon contact with soil due to rapid and strong adsorption (Wang et al., 2019). During the adsorption process, soil particles, including organic matter and clay minerals, play a dominant role in binding PQ (Knight and Tomlinson 1967; Burns *et al.*, 1973). The strong binding impedes the leaching of paraquat, and inhibits its breakdown or utilization by microorganisms in the soil solution (Roberts et al., 2002; Gondar *et al.*, 2012), leading to its persistence and potential entry into the food chain through biomagnification, ultimately posing a health risk to humans and mammals upon long-term exposure (Pateiro-Moure et al., 2009; Frimpong et al., 2018). Research indicates that the immobility and persistence of PQ in soil is attributed primarily to its adsorption by clay, rather than organic matter (Khan, 1974; Senesi et al., 1995; Bromilow, 2004). It was found that the adsorption capacity and binding strength of PQ on swelling clay (e.g. montmorillonite) far outweighs that on non-swelling clay (e.g. kaolinite) (e.g. Weber and Weed 1968). This is due to attractive electrostatic interactions between the negatively charged clay layers and the positively charged PQ.

Several scholars have conducted experimental studies on the adsorption of PQ on montmorillonite (Mnt) (Weber et al., 1965; Knight and Denny, 1970; Tsai et al., 2003; Tsai et al., 2004; Muhamad et al., 2011). The results obtained from these studies have revealed that exposure time has no significant impact on the adsorption of PQ on montmorillonite. On the other hand, solution pH and alkali metal ion concentration have a substantial effect on the adsorption process. Regarding the arrangement of PQ in the montmorillonite interlayer, previous studies have demonstrated that PQ formed a monolayer in parallel with montmorillonite layers in the anhydrous state (Knight and Denny, 1970; Raupach et al., 1979). However, the structures and dynamics of hydrated PQ-Mnt are yet to be explored.

Over the past 30 years, molecular simulation has shown unique advantages in uncovering the microstructure and dynamics of cations-clay and organic-clay systems, providing an important complement to experiments (Cygan et al., 2004a; Greenwell et al., 2005; Liu et al., 2007; Cygan et al., 2009; Liu et al., 2009; Zhu et al., 2012a; Ngouana and Kalinichev, 2014; Teich-McGoldrick et al., 2015; Scholtzová, 2016; Scholtzová, 2020; Cygan et al., 2021). Various force fields have been utilized to describe the interactions between herbicides and clay minerals. For example, Cosoli et al. (2010) employed the COMPASS force field to investigate the diffusion coefficient of atrazine herbicides in a saturated sand model. The results matched the experimental

results obtained by Helmke et al. (2005). The CHARMM (Brooks et al., 2009) force field and INTERFACE (Heinz et al., 2013) force field, which describe organic materials and inorganic materials, respectively, were adopted to probe the adsorption mechanisms of PQ and glyphosate on montmorillonite (Wang et al., 2019). By designing the variation in the protonation state of siloxane groups on the clay mineral surface at pH2 and pH7, and analyzing the herbicides' residence time on the surface under different pH conditions, Wang et al. (2019) discerned that the interlayer adsorption configuration of PQ remains unaffected by pH fluctuations. In the study conducted by Zhu et al. (2012a), ClayFF (Cygan et al., 2004b) and CVFF (Dauber-Osguthorpe et al., 1988) force fields were employed to investigate the adsorption of tetrachlorodibenzo-p-dioxin on tetramethylammonium and tetrapropylammonium modified montmorillonite. The findings indicated that dioxin exhibited a stronger interaction with tetra-alkylammonium species than with the clay surfaces. Additionally, the calculated adsorption energy of dioxin on the montmorillonite surface was comparable to that obtained from *ab initio* calculations (Austen et al., 2007). These results suggest that the combined ClayFF–CVFF force field is suitable for herbicide–montmorillonite systems.

The aim of this study was to characterize in detail the microscopic structures and mobility of PQ–Mnt. Systematic molecular dynamics simulations were performed for the PQ–Mnt systems with varying levels of water content. The swelling curves and swelling thermodynamics were obtained. The interlayer configurations of PQ and water molecules as well as PQ's mobility at different levels of water contents were characterized. The findings in the present study provide an atomic-level understanding for the environmental fate of PQ in soils.

Materials and methods

Models

Two montmorillonite models with different chemical compositions were built in this study. One had the same composition with Ilari et al. (2021), i.e. $Na_{0.84}[Si_{7.74}Al_{0.26}][Al_{2.88}Fe^{3+}_{0.54}Mg_{0.58}]O_{20}(OH)_4$ (denoted as 0.84-Mnt). The other was a common Fe^{3+}-free montmorillonite with a chemical formula of $Na_{1.0}[Si_8][Al_{3.0}Mg_{1.0}]O_{20}(OH)_4$ (denoted as 1.0-Mnt).

The supercell used in this study consisted of two clay platelets with each containing 24 unit cells: six in the *x*-dimension and four in the *y*-dimension (Fig. 1a,b). In the 0.84-Mnt system,

14 Mg^{2+} for Al^{3+} and 13 Fe^{3+} for Al^{3+} isomorphic substitutions in octahedral sheet and 6 Al^{3+} for Si^{4+} isomorphic substitutions in tetrahedral sheet were introduced in each layer, resulting in a layer charge density of –0.84 e/unit cell. In the 1.0-Mnt system, 24 isomorphic substitutions of Mg^{2+} for Al^{3+} in octahedral sheet were imposed in each layer, which resulted in a layer charge density of -1.0 e/unit cell. The isomorphic substitutions obey Loewenstein's rule, i.e. two substitution sites cannot be adjacent (Loewenstein 1954). Figure 1c shows the molecular structure of PQ cation $(C_{12}H_{14}N_2)^{2+}$. Initially, we placed 8 PQ cations randomly in each interlayer region of the 0.84-Mnt system (denoted as PQ-0.84-Mnt) according to the experimental loadings in Ilari et al. (2021). The samples measured in the experiment are considered to be anhydrous due to the drying process. Na^+ were used to compensate the net charges of the system. For the 1.0-Mnt system, we placed 12 PQ cations randomly in each interlayer region to compensate the net layer charge, denoted as PQ-1.0-Mnt. To study the effect of water content on the interlayer structure, a different number of water molecules were inserted into the interlayer region of PQ-1.0-Mnt (N_{water}=~0–600). For reference purposes, the water contents were converted to mg_{water}/g_{clay}, e.g. the water content for N=600 is 555 mg_{water}/g_{clay}, and the system is thus denoted as PQ-555. The compositions of paraquat-0.84-Mnt and paraquat-1.0-Mnt systems are shown in Table S1.

Computational details

All molecular dynamics simulations (MD) were carried out using the LAMMPS package (Plimpton, 1995). Clayff-CVFF was employed to describe the interactions in the systems. The partial charges of PQ (Table S1; Fig. S1) were obtained using the charge equilibration method (QEq) (Rappe and Goddard, 1991). The flexible single point charge (SPC) water model (Berendsen et al., 1981; Cygan et al., 2004b) was used to describe the water molecule. A 10.0 Å cut-off was used for the short-range interactions. The long-range electrostatic interactions were calculated using the Ewald summation method (Frenkel and Smit, 2002) and the number of K-space vectors was determined to reach a precision of 1.0×10^{-4}.

The isothermal-isobaric (constant particle number, pressure, and temperature; NPT) simulations were performed at 298K and 1 atm for 20 ns to obtain the basal spacing (Fig. S2). The equilibrium was confirmed by monitoring the evolution of simulation box and energy. Nosé-Hoover thermostat and barostat for temperature and pressure controls were used in this
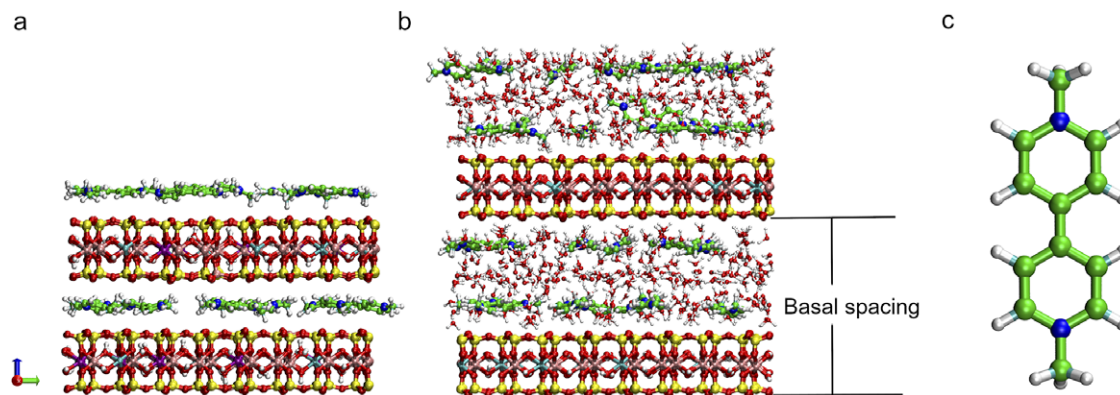
Figure 1. (a) Snapshot of the anhydrous PQ-0.84-Mnt; (b) snapshot of the paraquat-1.0-Mnt at 278 mg_{water}/g_{clay}; (c) structure of paraquat cation. Key: C, green; N, blue; H, white; O, red; Si, yellow; Mg, cyan; Al, pink; Fe, violet.

study, and the coupling constants were set to 0.1 ps and 1.0 ps, respectively. The equilibrium was checked by monitoring the evolution of simulation box and energy. The microscopic structures, immersion energy and dynamics of interlayer species were obtained from a 30 ns production run in the canonical ensembles (constant particle number, volume, and temperature; NVT) at 298K following the previous NPT simulations. In all simulations, the time step was set to 0.5 fs and an interval of 500 fs was used to record trajectories. All atoms were allowed to move freely.

Data analysis

The distribution of interlayer species in space is characterized by the atomic number density distribution along the z direction (normal to the clay basal plane), which is calculated by averaging the NVT trajectories. Consider the plane where the oxygen atoms in the silicon-oxygen ring at the bottom of the montmorillonite layer are as the starting plane ($z=0$).

The formula for distribution of species number density between layers is as follows:

$$\rho(z) = \frac{\langle N\left(z - \frac{\Delta z}{2}, z + \frac{\Delta z}{2}\right)\rangle}{\Delta z \times S}. \quad (1)$$

Here $N\left(z - \frac{\Delta z}{2}, z + \frac{\Delta z}{2}\right)$ is the average number of atoms appearing in the height interval $\left(z - \frac{\Delta z}{2}, z + \frac{\Delta z}{2}\right)$ ($\Delta z = 0.2$ Å in this work).

The self-diffusion coefficient D of interlayer species can be obtained using the Einstein relationship (Allen & Tildesley, 1987; Chang et al., 1997):

$$\frac{1}{N}\sum_{i=1}^{N}\langle |r_i(t) - r_i(0)|^2\rangle = 2dDt, \quad (2)$$

where N is the number of atoms, $r_i(t)$ is the center-of-mass position of the ith atom at time t, and d is the diffusion dimension. For example, $d = 3$ represents the total coefficient, and $d = 1$ represents the coefficient components in the x, y, and z directions. The left-hand side of Eqn (2) is the mean square displacement term (MSD). The components of MSD in each individual direction are denoted as XX, YY, and ZZ. The motion parallel to the x–y plane (denoted as ||) is calculated as (XX+YY)/2. The standard error was taken as the error. The self-diffusion coefficients were calculated from the MSD within 2 ns intervals in the linear portion of the MSD curve, which spanned from 2 ns to 18 ns. We divided this 16 ns period into eight equal segments and utilized these segments to calculate the standard error. Given that simulation size may have an impact on the diffusion coefficient, we utilized the correction method proposed by Simonnin et al. (2017) in our study. The interlayer water viscosity, as provided by Ho et al. (2020), was selected for calculation purposes. In the PQ-185 systems, the original self-diffusion coefficient of water was 3.388×10^{-10} m^2 s^{-1} with a correcting amplitude of -5.3×10^{-12} m^2 s^{-1}. In the PQ-278 systems, the original self-diffusion coefficient of water was 5.663×10^{-10} m^2 s^{-1} with a correcting amplitude of -6.7×10^{-12} m^2 s^{-1}. The magnitude of the correction in both systems is considered negligible and can be disregarded.

Results and Discussion

Swelling behaviors

In the simulated swelling curve of PQ-1.0-Mnt (Fig. 2), the experimental value for the anhydrous PQ-0.84-Mnt is also shown

for comparison. It can be observed that the experimental value is very close to our calculated basal spacing, i.e. 12.5 Å *vs* 12.7 Å. This agreement indicates that the ClayFF-CVFF force field can describe the swelling behavior of the PQ-Mnt system. Swelling thermodynamics is described using the immersion energy (Boek et al., 1995; Smith, 1998), which is defined as:

$$Q = U(N) - U(N_0) - (N - N_0)U_{bulk},$$

where $U(N)$ is the potential energy of hydrated montmorillonite, $U(N_0)$ is the energy of the reference state (370 mg$_{water}$/g$_{clay}$ in this study), and U_{bulk} is the mean interaction potential of the bulk flexible SPC water (-41.12 kJ mol^{-1}) (Teleman et al., 1987), which was calculated from the simulation of a pure water system. The immersion energy Q represents the energy released when the system with N water molecules is transformed into the reference state through water absorption from the bulk water.
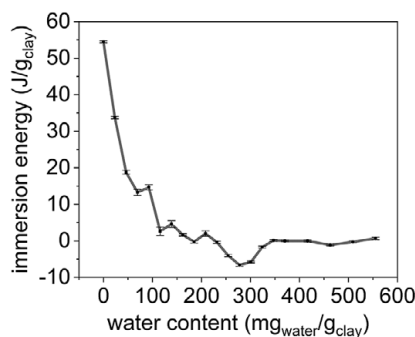
In the calculated immersion energy curve of the PQ-1.0-Mnt systems (Fig. 3), two minima can be identified on the curve: local minimum at 185 mg$_{water}$/g$_{clay}$ (200 water molecules in each interlayer region) and global minimum at 278 mg$_{water}$/g$_{clay}$ (300 water molecules in each interlayer region). These minima suggest that PQ-1.0-Mnt with the corresponding water contents are thermodynamically stable and could exist in natural or experimental conditions. Therefore, these two hydrated systems and the anhydrous system were selected to investigate the interlayer structures and dynamics in the following sections. The energy barrier for the transformation from the 185 mg$_{water}$/g$_{clay}$ state to the 278 mg$_{water}$/g$_{clay}$ state was estimated to be ~3.0 J g$_{clay}^{-1}$, indicating that PQ-1.0-Mnt can swell. (Information on the interlayer structure when the water content was <100 mg$_{water}$/g$_{clay}$ is provided in the Supplementary material; see Fig. S3.)

Interlayer structure

To investigate the arrangement of interlayer species, we calculated the atomic number density along the z-axis direction, which was obtained by averaging the density in the two interlayer regions. The PQ cations were represented by N and C atoms, and water molecules were represented by O atoms. In the anhydrous system, PQ presented a sharp peak in the density profile (Fig. 4a), suggesting that PQ formed a monolayer, with the bipyridine ring plane parallel to the montmorillonite surface (Fig. 5a). In PQ-185 and PQ-278 systems, three peaks can be identified for water molecules (Fig. 4b,c), suggesting a triple-layer-like structure. PQ cations show two sharp peaks in the two hydrated states. It was found from the trajectory that PQs are in direct contact with the
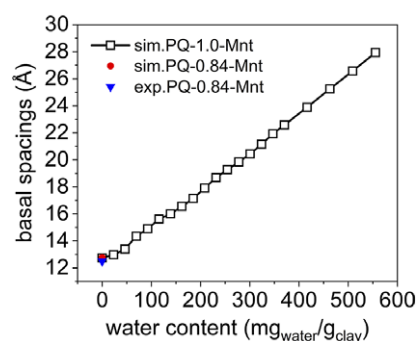
Figure 2. Simulated swelling curve of PQ-1.0-Mnt. For comparison, the calculated basal spacing for the anhydrous PQ-0.84-Mnt is also presented alongside the corresponding experimental value (Ilari et al., 2021).

Figure 3. Simulated immersion energy curve of paraquat-1.0-Mnt. The statistical error was estimated as the standard error of average values obtained from 10 evenly divided fragments of the trajectory (each spanning 3 ns intervals).

clay mineral surface, and there are no water molecules between them.

As presented above, PQ cations adopted a parallel orientation to the clay surface in both anhydrous and hydrated states. The PQ molecules were nearly parallel to the clay surface. In all systems, the angles between the two PQ pyridine rings peaked at approximately 14–30° (Fig. 6). Due to the influence of clay surfaces and water molecules on PQ cations, the angle between the pyridine rings deviated from the equilibrium of 30° (Mendes et al., 2020; Hou and Wang, 2021; Macii et al., 2021). The hydration shell of PQ in hydrated PQ-Mnts were depicted using the spatial distribution function of water around PQ (Fig. 7). In both hydration states, there is no water distribution between PQ molecules and montmorillonite basal surface, indicating that PQ is in direct contact with montmorillonite. However, no correlation between clay substitutions and PQ location was found from the trajectories. In PQ-185, no water distributed above PQ molecules along the z direction (the

hydration shell exists only in the xy plane), which suggests that PQ is also in direct contact with other PQ molecule. Together with the equilibrium structure, this observation suggests that PQ molecules formed stable π-π stacking in PQ-185. In PQ-278, the hydration shell is closed above the PQ molecule, which is consistent with the density distribution curve in Fig. 4c where the PQ molecules were separated by a water layer.

Mobility of interlayer species

To investigate the mobility of PQ, we calculated the self-diffusion coefficient of PQ at different water contents (Fig. 8) (see Supplementary material for more details). The diffusion coefficients of PQ at these water contents are all of the magnitude of 10^{-13} to 10^{-11} m^2 s^{-1}. They are much smaller than the self-diffusion coefficient (magnitude of 10^{-9}–10^{-8} m^2 s^{-1}) of various polycyclic aromatic hydrocarbons (e.g. PAHs, including naphthalene, anthracene, chrysene, and benzopyrene) intercalated in clay minerals in a wide range of water contents (Chen and Hu, 2022; Zhao et al., 2023), and it is also significantly smaller than the self-diffusion coefficient of PQ in bulk water (~10^{-10} m^2 s^{-1}).

As PQ cations almost only move in the xy plane direction, the self-diffusion coefficients diagram (Fig. 8) revealed that the self-diffusion coefficient ($D_{\parallel}$) were similar for the anhydrous state and PQ-185, and both were significantly smaller than that at PQ-278 that lacked π-π stacking interactions. These results indicate that PQ has very limited movement in the interlayer region and can be effectively trapped by montmorillonite. It is consistent with previous conclusion (e.g. Smith and Mayfield, 1978; Leonard et al., 1979; Ouyang et al., 2004; Amondham et al., 2006) that the transport of paraquat is extremely limited in clay-rich soils. In the PQ-175 and PQ-278 systems, the self-diffusion coefficients of water molecules increased with water content, and was much smaller than the mobility of bulk water (Mark and Nilsson, 2001) (Fig. 9).
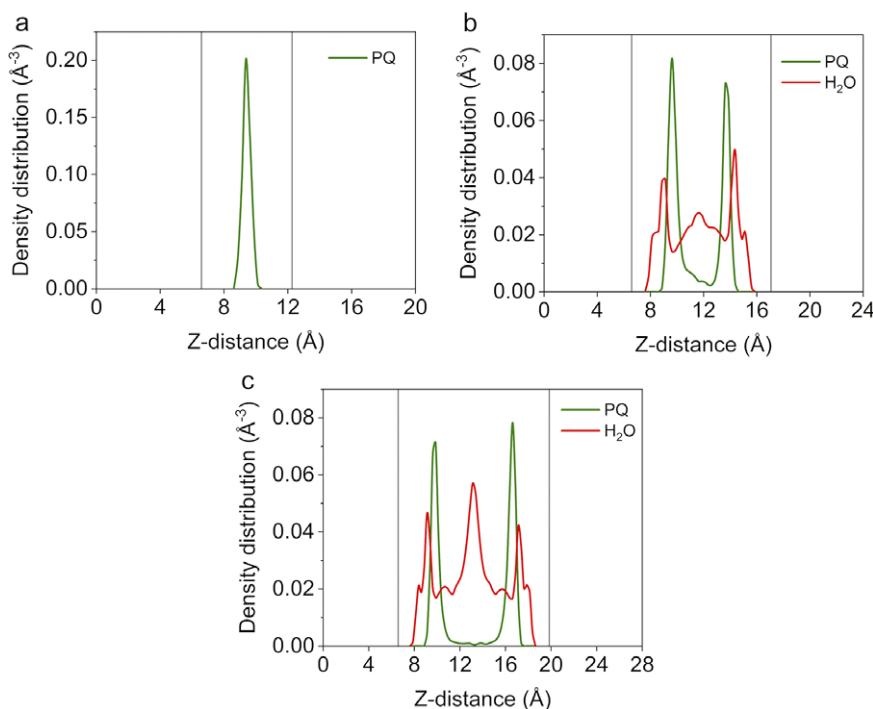
Figure 4. Z-density distribution of the paraquat and water molecules in the PQ-1.0-Mnt systems with different water contents (the gray line represents the location of the inner surface of the montmorillonite layer). (a) PQ-0 system; (b) PQ-185 system; (c) PQ-278 system.
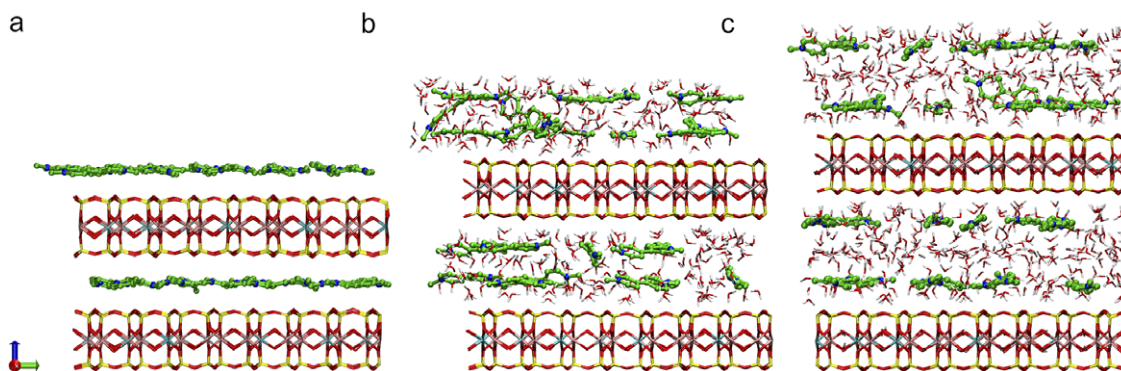
Figure 5. Snapshots of the PQ-1.0-Mnt systems at different water contents. (a) PQ-0 system; (b) PQ-185 system; (c) PQ-278 system. Key: C, green; N, blue; H, white; O, red; Si, yellow; Mg, cyan; Al, pink. Hydrogen atoms of paraquat molecules are not shown for clarity.
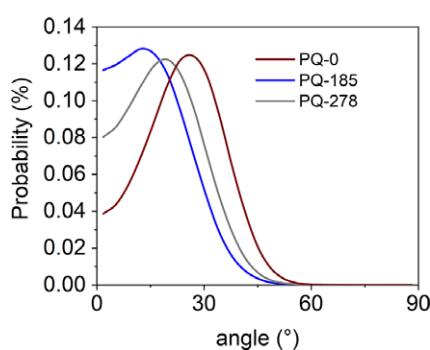
Figure 6. Probability distribution of angles between pyridine rings connected to each other within PQ cations in different systems.

Conclusion

Paraquat is used widely in agriculture production, and poses a health risk to humans due to its long-term stability in soils. In this study, molecular dynamics simulations were conducted to explore the structure and dynamics of PQ in the interlayer space of montmorillonite. Two stable hydration states were identified, one with a water content of 185 mg_{water}/g_{clay} and the other of 278 mg_{water}/g_{clay}, with the latter being the most stable. The interlayer structures and mobility of PQ in the stable hydration and anhydrous states were obtained. It was found that PQs were in direct contact with clay surfaces in both anhydrous and hydrated states. At the water content of 185 mg_{water}/g_{clay}, PQs formed π-π stacking while at the water content of 278 mg_{water}/g_{clay}, the PQs were separated by a layer of water. The self-diffusion coefficient of
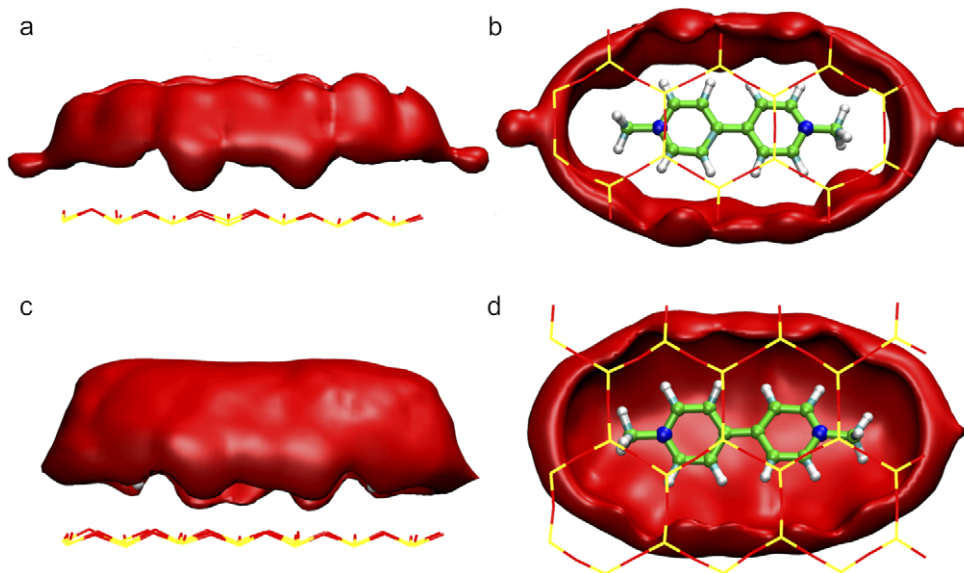

Figure 7. The spatial distribution maps of water molecules (hydration shell) around PQ on the lower surface of the montmorillonite. (a) Front view for PQ-185 system; (b) bottom view for PQ-185 system; (c) front view for PQ-278 system; (d) bottom view for PQ-278 system. Key: C, green; N, blue; H, white; Si, yellow; Mg, cyan; Al, pink; O, red. Clay surfaces are represented by thin lines.

Moreover, these coefficients were found to be within the same order of magnitude as the self-diffusion coefficient of interlayer water in Na and Ca-montmorillonite with two or three layers of water (Greathouse et al., 2015; Zhang et al., 2014).

PQ ranges from 10^{-12} to 10^{-11} $m^2\ s^{-1}$, with a slightly greater value observed at the high water content. Notably, the diffusivity of PQ is significantly smaller than that of other aromatic organic compounds. The findings presented in this study provide an
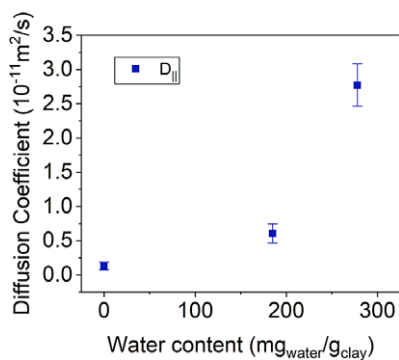
Figure 8. The self-diffusion coefficient ($D_\parallel$) of PQ in PQ-1.0-Mnt at different water contents.
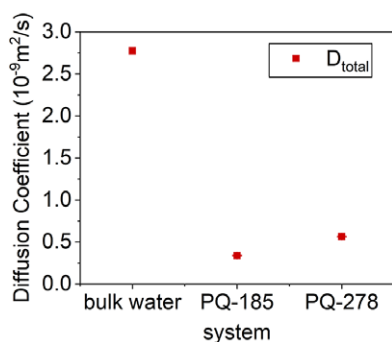
Figure 9. The self-diffusion coefficient (D_{total}) of water in PQ-185, PQ-278, and bulk water.

atomic-level insight into the stability of PQ in soils and forms a microscopic basis for development of efficient remediation strategy.

References

Allen, M.P. & Tildesley, D. J. (1987). *Computer Simulation of Liquids.* Clarendon Press: Oxford, UK.

Amondham W., Parkpian, P., Polprasert, C., DeLaune, D.R., & Jugsujinda, A. (2006). Paraquat adsorption, degradation, and remobilization in tropical soils of Thailand. *Journal of Environmental Science and Health Part B*, *41*, 485–507.

Austen, K.F., White, T.O.H., Marmier, A., Parker, S., Artacho, E., & Dove, M.T. (2007). Electrostatic versus polarization effects in the adsorption of aromatic molecules of varied polarity on an insulating hydrophobic surface. *Journal of Physics: Condensed Matter*, *20*, 035215.

Berendsen, H.J.C., Postma, J.P.M., van Gunsteren, W.F., & Hermans, J. (1981). Interaction models for water in relation to protein hydration. In B. Pullman (ed), *Intermolecular Forces* (pp. 331–342). Riedel: Dordrecht, Netherlands.

Boek, E.S., Coveney, P. V., & Skipper, N. T. (1995). Monte Carlo molecular modeling studies of hydrated Li-, Na-, and K-smectites: understanding the role of potassium as a clay swelling inhibitor. *Journal of the American Chemical Society*, *117*, 12608–12617.

Bromilow, R.H. (2004). Paraquat and sustainable agriculture. *Pest Management Science*, *60*, 340–349.

Brooks, B.R., Brooks III, C.L., MacKerell Jr, A.D., Nilsson, L., Petrella, R.J., Roux, B., Won, Y., Archontis, G., Bartels, C., Boresch, S., Caflisch, A., Caves, L., Cui, Q., Dinner, A.R., Feig, M., Fischer, S., Gao, J., Hodoscek, M., Im, W., Kuczera, K., Lazaridis, T., Ma, J., Ovchinnikov, V., Paci, E., Pastor, R.W., Post, C.B., Pu, J.Z., Schaefer, M., Tidor, B., Venable, R.M., Woodcock, H.L., Wu, X., Yang, W., York, D.M., & Karplus, M. (2009). CHARMM: the biomolecular simulation program. *Journal of Computational Chemistry*, *30*, 1545–1614.

Burns, I.G., Hayes, M.H.B., & Stacey, M. (1973). Some physico-chemical interactions of paraquat with soil organic materials and model compounds. *Weed Research*, *13*, 79–90.

Chang, F.-R.C., Skipper, N.T., & Sposito, G. (1997). Monte Carlo and molecular dynamics simulations of interfacial structure in lithium-montmorillonite hydrates. *Langmuir*, *13*, 2074–2082.

Chen, Z., & Hu, L. (2022). Adsorption of naphthalene on clay minerals: a molecular dynamics simulation study. *Materials*, *15*, 5120.

Cosoli, P., Fermeglia, M., & Ferrone, M. (2010). Molecular simulation of atrazine adhesion and diffusion in a saturated sand model. *Soil and Sediment Contamination*, *19*, 72–87.

Cygan, R.T., Guggenheim, S., & van Groos, A.F.K. (2004a). Molecular models for the intercalation of methane hydrate complexes in montmorillonite clay. *Journal of Physical Chemistry B*, *108*, 15141–15149.

Cygan R.T., Liang J.J., & Kalinichev A.G. (2004b). Molecular models of hydroxide, oxyhydroxide, and clay phases and the development of a general force field. *Journal of Physical Chemistry B*, *108*, 1255–1266.

Cygan, R.T., Greathouse, J.A., Heinz, H., & Kalinichev, A.G. (2009). Molecular models and simulations of layered materials. *Journal of Materials Chemistry*, *19*, 2470–2481.

Cygan, R.T., Greathouse, J.A., & Kalinichev, A.G. (2021). Advances in ClayFF molecular simulation of layered and nanoporous materials and their aqueous interfaces. *Journal of Physical Chemistry C*, *125*, 17573–17589.

Dauber-Osguthor P., Roberts, A.V., Osguthorpe, J.D., Wolff, J., Genest, M. & Hagler, T.A. (1988) Structure and energetics of ligand binding to proteins: *E. coli* dihydrofolate reductase-trimethoprim, a drug-receptor system. *Proteins: Structure, Function and Genetics*, *4*, 31–47.

Frenkel, D., & Smit, B. (2002) *Understanding Molecular Simulation* (2nd edn). Academic Press: New York, USA.

Frimpong, J.O., Ofori, E.S.K., Yeboah, S., Marria, D., Offeia, B.K., Apaataha, F., Sintima, J.O., Ofori-Ayeh, E., & Osae, M. (2018). Evaluating the impact of synthetic herbicides on soil dwelling macrobes and the physical state of soil in an agro-ecosystem. *Ecotoxicology and Environmental Safety*, *156*, 205–215.

Gondar, D., López, R., Antelo, J., Fiol, S., & Arce, F. (2012). Adsorption of paraquat on soil organic matter: effect of exchangeable cations and dissolved organic carbon. *Journal of Hazardous Materials*, *235–236*, 218–223.

Greathouse, J.A., Hart, D.B., Bowers, G.M., Kirkpatrick, R.J., & Cygan, R.T. (2015). Molecular simulation of structure and diffusion at smectite–water interfaces: using expanded clay interlayers as model nanopores. *Journal of Physical Chemistry C*, *119*, 17126–17136.

Greenwell, H.C., Jones, W., Coveney, P.V, & Stackhouse, S. (2005). On the application of computer simulation techniques to anionic and cationic clays: a materials chemistry perspective. *Journal of Materials Chemistry*, *16*, 708–723.

Heinz, H., Lin, T.J., Mishra, R.K., & Emami, F.S. (2013). Thermodynamically consistent force fields for the assembly of inorganic, organic, and biological nanostructures: the INTERFACE force field. *Langmuir*, *29*, 1754–1765.

Helmke, M.F., Simpkins, W.W., & Horton, R. (2005). Fracture-controlled nitrate and atrazine transport in four Iowa till units. *Journal of Environmental Quality*, *34*, 227–236.

Ho, T.A., Wang, Y., Jové Colón, C.F., & Coker, E.N. (2020) Fast advective water flow through nanochannels in clay interlayers: implications for moisture transport in soils and unconventional oil/gas production. *ACS Applied Nano Materials*, 3, 11897–11905.

Hou, H., & Wang, B. (2021). Solvent-dependent mechanistic aspects for the redox reaction of paraquat in basic solution. *International Journal of Quantum Chemistry*, 121, e26757.

Ilari, R., Etcheverry, M., Waiman, V.C., & Zanini, G. (2021). A simple cation exchange model to assess the competitive adsorption between the herbicide paraquat and the biocide benzalkonium chloride on montmorillonite. *Colloids and Surfaces A: Physicochemical and Engineering Aspects*, 611, 125797.

Khan, S.U. (1974). Determination of diquat and paraquat residues in soil by gas Chromatography. *Journal of Agricultural and Food Chemistry*, 22, 863–867.

Knight, B.A.G., & Tomlinson, T.E. (1967). The interaction of paraquat (1:1 0-dimethyl 4:4 0-dipyridylium dichloride) with mineral soils. *Journal of Soil Science*, 18, 233–243.

Knight, B.A.G., & Denny, P.J. (1970). The interaction of paraquat with soil: adsorption by an expanding lattice clay mineral. *Weed Research*, 10, 40–48.

Leonard, R.A., Langdale, G.W., & Fleming, W.G. (1979). Herbicide runoff from upland Piedmont watersheds – data and implications for modeling pesticide transport. *Journal of Environmental Quality*, 8, 223–229.

Liu, X.D., Lu, X.C., Wang, R.C., Zhou, J.H., & Xu, X.S. (2007). Interlayer structure and dynamics of alkylammonium-intercalated smectites with and without water: a molecular dynamics study. *Clays and Clay Minerals*, 55, 554–564.

Liu, X.D., Lu, X.C., Wang, R.C., Zhou, H.Q., & Xu, S.J. (2009). Molecular dynamics in-sight into the cointercalation of hexadecyltrimethyl-ammonium and acetate ions into smectites. *American Mineralogist*, 94, 143–150.

Loewenstein, W. (1954). The distribution of aluminum in the tetrahedra of silicates and aluminates. *American Mineralogist*, 39, 92–96.

Macii, F., Detti, R., Bloise, F.R., Giannarelli, S., & Biver, T. (2021). Spectroscopic analysis of the binding of paraquat and diquat herbicides to biosubstrates. *International Journal of Environmental Research and Public Health*, 18, 2412.

Mark, P., & Nilsson. L. (2001). Structure and dynamics of the TIP3P, SPC, and SPC/E water models at 298K. *Journal of Physical Chemistry A*, 105, 9954–9960.

Mendes, R.A., de Freitas, R.G., Brown, A., & de Souza, G.L.C. (2020). Exploring ground and low-lying excited states for diquat, paraquat, and dipyridyl isomers. *Journal of Photochemistry & Photobiology A: Chemistry*, 402, 112817.

Muhamad, H., Ismail, B.S., Sameni, M., & Mat, N. (2011). Adsorption study of ^{14}C-paraquat in two Malaysian agricultural soils. *Environmental Monitoring and Assessment*, 176, 43–50.

Ngouana W, B.F., & Kalinichev, A.G. (2014). Structural arrangements of isomorphic substitutions in smectites: molecular simulation of the swelling properties, interlayer structure, and dynamics of hydrated Cs–montmorillonite revisited with new clay models. *Journal of Physical Chemistry C*, 118, 12758–12773.

Ouyang, Y., Mansell, R.S., & Nkedi-Kizza, P. (2004). Displacement of paraquat solution through a saturated soil column with contrasting organic matter content. *Bulletin of Environmental Contamination & Toxicology*, 73, 725–731.

Pateiro-Moure, M., Nóvoa-Munoz, J.C., Arias-Estévez, M., López-Periago, E., Martínez-Carballo, E., & Simal-Gándara, J. (2009). Quaternary herbicides retention by the amendment of acid soils with a bentonite-based waste from wineries. *Journal of Hazardous Materials*, 164, 769–775.

Plimpton, S.J. (1995). Fast parallel algorithms for short-range molecular dynamics. *Journal of Computational Physics*, 117, 1–19.

Rappe, K.A., & Goddard III, W.A. (1991). Charge equilibration for molecular dynamics simulations. *The Journal of Physical Chemistry*, 95, 3358–3363.

Rashidipour, M., Maleki, A., Kordi, S., Birjandi, M., Pajouhi, N., Mohammadi, E., Heydari, R., Rezaee, R., Rasoulian, B., & Davari, B. (2019). Pectin/chitosan/tripolyphosphate nanoparticles: efficient carriers for reducing soil sorption, cytotoxicity, and mutagenicity of paraquat and enhancing its herbicide activity. *Journal of Agricultural and Food Chemistry*, 67, 5736–5745.

Raupach, M., Emerson, W.W., & Slade, P.G. (1979). The arrangement of paraquat bound by vermiculite and montmorillonite. *Journal of Colloid and Interface Science*, 69, 398–408.

Roberts, T.R., Dyson, J.S., & Lane, M.C.G. (2002). Deactivation of the biological activity of paraquat in the soil environment: a review of long-term environmental fate. *Journal of Agricultural and Food Chemistry*, 50, 3623–3631.

Santos, M.S.F., Schaule, G., Alves, A., & Madeira, L.M. (2013). Adsorption of paraquat herbicide on deposits from drinking water networks. *Chemical Engineering Journal*, 229, 324–333.

Scholtzová, E., Madejová, J., Jankovič, L., & Tunega, D. (2016). Structural and spectroscopic characterization of montmorillonite intercalated with N-butylammonium cations (N = 1-4) – modeling and experimental study. *Clays and Clay Minerals*, 64, 401–412.

Scholtzová, E., 2020. Computational modeling of nanoclays. In G., Cavallaro, R., Fakhrullin & P., Pasbakhsh (eds), *Micro and Nano Technologies Series, Clay Nanoparticles Properties and Applications* (pp. 139–166). Elsevier: Netherlands.

Senesi, N., D'Orazio, V., & Miano, T.M. (1995). Adsorption mechanisms of s-triazine and bipyridylium herbicides on humic acids from hop field soils. *Geoderma*, 66, 273–283.

Smith, D.E. (1998). Molecular computer simulations of the swelling properties and inter-layer structure of cesium montmorillonite. *Langmuir*, 14, 5959–5967.

Simonnin, P., Noetinger, B., Nieto-Draghi, C., Marry, V., & Rotenberg, B. (2017). Diffusion under confinement: hydrodynamic finite-size effects in simulation. *Journal of Chemical Theory and Computation*, 13, 2881–2889.

Smith, E.A., & Mayfield, C.I. (1978). Paraquat: determination, degradation, and mobility in soil. *Water, Air, and Soil Pollution*, 9, 439–452.

Teich-McGoldrick, S.L., Greathouse, J.A., Jové-Colón, C.F., Cygan, R.T. (2015). Swelling properties of montmorillonite and beidellite clay minerals from molecular simulation: comparison of temperature, interlayer cation, and charge location effects. *Journal of Physical Chemistry B*, 119, 20880–20891.

Teleman, O., Jönsson, B., & Engström, S. (1987). A molecular dynamics simulation of a water model with intramolecular degrees of freedom. *Molecular Physics*, 60, 193–203.

Tsai, W.T., Lai, C.W., & Hsien, K.J. (2003). The effects of pH and salinity on kinetics of paraquat sorption onto activated clay. *Colloids and Surfaces A: Physicochemical and Engineering Aspects*, 224, 99–105.

Tsai, W.T., Lai, C.W., & Hsien, K.J. (2004). Adsorption kinetics of herbicide paraquat from aqueous solution onto activated bleaching earth. *Chemosphere*, 55, 829–837.

Wang, M., Orr, A.A., He, S., Dalaijamts, C., Chiu, W.A, Tamamis, P., & Phillips, T.D. (2019). Montmorillonites can tightly bind glyphosate and paraquat reducing toxin exposures and toxicity. *ACS Omega*, 4, 17702–17713.

Weber, J.B., Perry, P.W., & Upchurch, R.P. (1965). The influence of temperature and time on the adsorption of paraquat, diquat, 2, 4-D and prometone by clays, charcoal, and an anion-exchange resin. *Soil Science Society of America Journal*, 29, 678–688.

Weber, J. B., & Weed, S.B. (1968). Adsorption and desorption of diquat, paraquat, and prometone by montmorillonitic and kaolinitic clay minerals. *Soil Science Society of America Journal*, 32, 485–487.

Zhao, N., Tan, Y., Zhang, X., Zhen, Z., Song, Q., Ju, F., & Ling, H. (2023). Molecular insights on the adsorption of polycyclic aromatic hydrocarbons on soil clay minerals. *Environmental Engineering Science*, 40, 105–113.

Zhu, J., Shen, W., Ma, Y., Ma, L., Zhou, Q., Yuan, P., Liu, D., & He H. (2012a). The influence of alkyl chain length on surfactant distribution within organo-montmorillonites and their thermal stability. *Journal of Thermal Analysis and Calorimetry*, 109, 301–309.

Zhang, L., Lu, X., Liu, X., Zhou, J., & Zhou, H. (2014) Hydration and mobility of interlayer ions of (nax, cay)-montmorillonite: a molecular dynamics study. *Journal of Physical Chemistry C*, 118, 29811–29821.